Korean J. Chem. Eng., **21**(1), 236-245 (2004)

Vacuum Swing Adsorption Process for the Separation of Ethylene/Ethane with $AgNO_3$/Clay Adsorbent

Jong-Ho Park, Sang-Sup Han, Jong-Nam Kim and Soon-Haeng Cho†

Korea Institute of Energy Research, 71-2, Jangdong, Yusungku, Daejeon 305-343, Korea
(*Received 5 August 2003 • accepted 27 November 2003*)

Abstract−The performance of the 4-bed and 3-bed VSA process using $AgNO_3$/clay adsorbent for the ethylene separation from C2 fractionator feed (83.56% C_2H_4, 16.44% C_2H_6) was investigated experimentally and theoretically. With the 4-bed VSA process, extremely high recovery of ethylene, over 99%, was obtained at ethylene purity of 99.8%. The recovery of the 3-bed process was lower about by 1% than that of the 4-bed VSA process. But, the productivity of the 3-bed VSA was higher about by 33% than that of the 4-bed VSA process. The productivity of the 3-bed VSA process was 3.7 mol/kg/hr at the ethylene purity of 99.8%. Effects of the rinse flow rate in the 3-bed VSA process were investigated by both experiment and simulation. The purity of ethylene was not significantly improved by the increase of the rinse flow rate after it reached 99.8%. At the rinse flow rate where the purity was 99.9%, the recovery became 70%. It might be attributed to the slow diffusion of ethane. According to the simulation, ethylene purity of over 99.9% could be obtained with recovery of over 90% only when the mass transfer rate of ethane is lower than 1.0×10^{-4} s^{-1} or higher than 0.2 s^{-1}. The productivity of the process could be improved by increasing the feed flow rate at the expense of the recovery. According to the simulation, at the feed flow rate of 5,000 ml/min, the productivity of 5.2 mol/kg/hr was obtained at the ethylene purity of 99.5%.

Key words: Ethylene, Ethane, π-Complexation, VSA, Separation, Productivity

INTRODUCTION

Ethylene is the most important building block in the petrochemical industry. Steam cracking of naphtha or ethane is the main route of the ethylene production. Separation of ethylene from the cracked gas is the essential step of ethylene production. The separations of ethylene from ethane and propylene from propane have been achieved conventionally by low temperature and/or high-pressure distillation. Therefore, the conventional process is one of the most energy intensive processes. For this reason, a number of researchers have been developing other separation processes, which can replace the distillation. Among them, separation based on π-complexation appears the most promising.

Separation via π-complexation is a sub-group of chemical complexation where the mixture is brought into contact with a second phase containing a complexing agent [Cotton and Wilkinson, 1966; King, 1987; Yang and Kikkinides, 1995]. Transition metals, i.e., from Sc to Cu, Y to Ag and La to Au in the periodic table or their ions can form π-bonds with unsaturated hydrocarbons (olefins). These metals or their ions can form the normal s bond to carbon and, in addition, the unique characteristics of the d orbitals in these metals or ions can form bonds with olefins in a nonclassical manner. This type of bonding is broadly referred to as π-complexation.

The early attempts for the separation of olefin/paraffin mixtures based on π-complexation employed liquid solutions containing silver (Ag^+) or cuprous (Cu^+) ions [Ho et al., 1988; Keller et al., 1992]. There have been a number of studies with gas-solid systems based on π-complexation [Gilliland et al., 1941; Hirai et al., 1985, 1992; Cen, 1991].

More recent efforts to find available sorbents and to prepare new sorbents for the separations of ethylene/ethane and propylene/propane by pressure swing adsorption, have appeared in the literature [Yang and Kikkinides, 1995; Chen and Yang, 1995; Wu et al., 1997; Rege et al., 1998, Ramachandran et al., 1998; Cho et al., 1999, 2000, 2001, 2002; Han et al., 1999; Choudary et al., 2002]. Especially, Yang et al. have prepared several kinds of new solid sorbents for selective light olefin adsorption over corresponding paraffin via π-complexation; Ag^+-exchanged resins, monolayered CuCl/γ-alumina, monolayered CuCl/pillared clays and monolayered $AgNO_3/SiO_2$.

Cho et al. [2000, 2001] recently prepared the adsorbent $AgNO_3$/clay for olefin separation. It has been successfully applied for the recovery of ethylene from LDPE off-gas with the 4-bed VSA process [Cho et al., 2002]. The study revealed that ethylene of over 99.95% could be produced with a recovery of 93%. However, the productivity of the process was 1.98 mol/kg/hr. Such a low productivity could be a barrier to commercialization.

In this study, a 3-bed VSA process using $AgNO_3$/clay is proposed and its performance is compared to the 4-bed VSA process. The VSA process is often applied when a component of the gas mixture is strongly adsorbed on the adsorbent [Choi et al., 2003]. If the 3-bed VSA process gives similar product recovery at a given purity, it will be more economical than the 4-bed VSA process. In addition, parametric studies with a diffusion rate of ethane and feed flow rate are performed. The role of the diffusion rate of the weakly adsorbed component into the adsorbent has not attracted much attention because it is usually faster than the strongly adsorbed component. When the diffusion rate of the weakly adsorbed compo-

†To whom correspondence should be addressed.
E-mail: soonhcho@kier.re.kr
‡This paper is dedicated to Professor Hyun-Ku Rhee on the occasion of his retirement from Seoul National University.

Table 1. Physical properties of the substrate and the prepared adsorbent

Material	$AgNO_3$/g-substrate [-]	Average pore size [A]	BET surface area [m^2/g]	Pore volume [cm^3/g]
Substrate (clay)	Nil	40.3	392	0.42
Prepared adsorbent	0.4	34.0	172	0.23

nent is high, high purity of the strongly adsorbed component is easily obtained by purging with the strongly adsorbed component. However, on the π-complexation adsorbent, the weakly adsorbed component often showed slower diffusion rate than the strongly adsorbed component [Choudary et al., 2002; Yang and Kikkinides, 1995; Cheng and Yang, 1995]. If this is the case, then the rinse step may not increase the purity of the strongly adsorbed component much. By simulations, the effects of the mass transfer coefficient are investigated.

EXPERIMENTAL

1. Adsorbent

The substrate used in the present study is granular Montmorillonite clay of 1.0-2.0 mm. Typical Montmorillonite clay contains a relatively large amount of magnesium oxide among various clays. The pore size distribution of these substrates exists predominantly in mesoporous region. The chemical used as a complexing agent was $AgNO_3$ (at least 99.8% purity) from Junsei Chemicals Co., Japan. The detailed preparation procedure of the adsorbent is found elsewhere [Cho et al., 2002].

The physical properties of the substrate and the prepared adsorbent are shown in Table 1. The amount of $AgNO_3$ dispersed on the clay adsorbent is 0.4 g/g clay. The BET surface area and the pore volume of $AgNO_3$/clay were about half of the original substrate.

2. Cycle Experiment

A vacuum swing adsorption unit was designed and manufactured to operate automatically. The schematic of this unit is shown in Fig. 1. The apparatus was composed of four beds [25 mm(ID)×1,000 mm(H)×4 beds] in which prepared $AgNO_3$/clay adsorbent was loaded. The adsorption pressure was controlled by the back pressure regulator installed in the product line. C2 fractionator feed (83.56% C_2H_4, 16.44% C_2H_6) for the experiment was supplied by the LG-petrochemical in a high pressure gas cylinder. Flow rates of product, rinse, and raffinate were measured by the mass flow meter and the data were automatically stored in a personal computer. Valve opening was controlled by PLC (programmable logic controller). Pressure and temperature were monitored in real time and stored to the computer. The concentrations of the product and raffinate stream were measured with a gas chromatography. Since the product was first stored in the large volume of surge tank and then flowed out of the tank, the measured product concentration was a volume averaged one.

Breakthrough experiments were performed by using one of the four columns. In the breakthrough experiment, the concentrations of ethylene and ethane were measured by a mass spectrometer, which enabled continuous measurement of both components.

3. Process Description

Two cycle configurations are compared in this study: 4-bed VSA and 3-bed VSA processes. The cycle configuration of the 4-bed VSA process is the same as that reported in a previous paper [Cho et al., 2002]. For comparison, cycle configurations and flow directions of the 4-bed and 3-bed VSA processes are shown in Fig. 2. In the 4-bed VSA process, the effluent of the rinse step is recycled

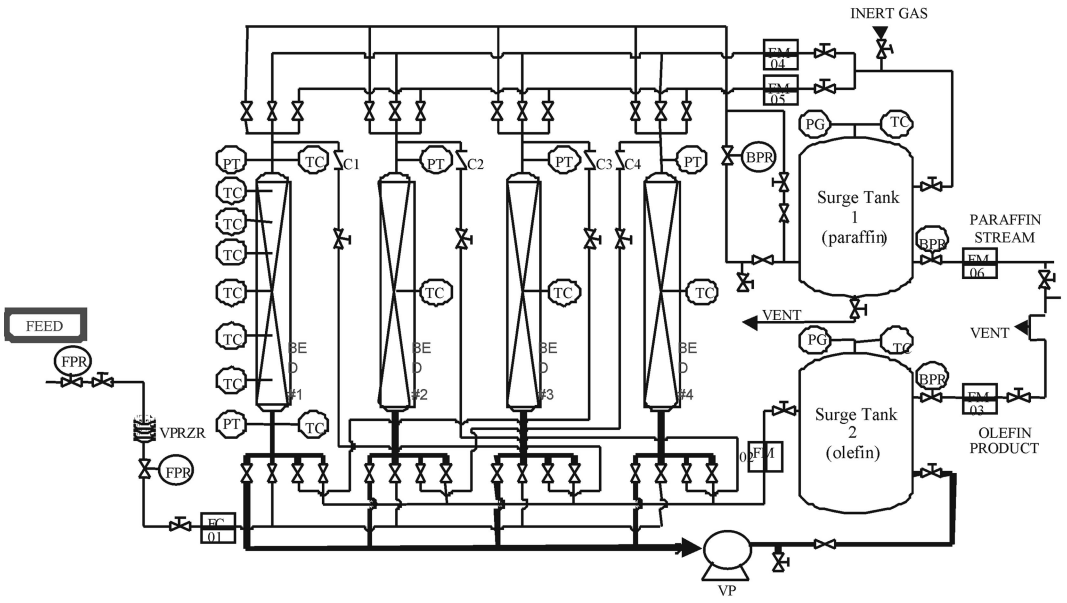

Fig. 1. Schematic diagram of the 4-bed and 3-bed VSA process.
PT: Pressure transmitter TC : Thermocouple BPR: Back pressure regulator FPR: Fore pressure regulator
FM: Mass flow meter VP: Vacuum pump FC: Mass flow controller

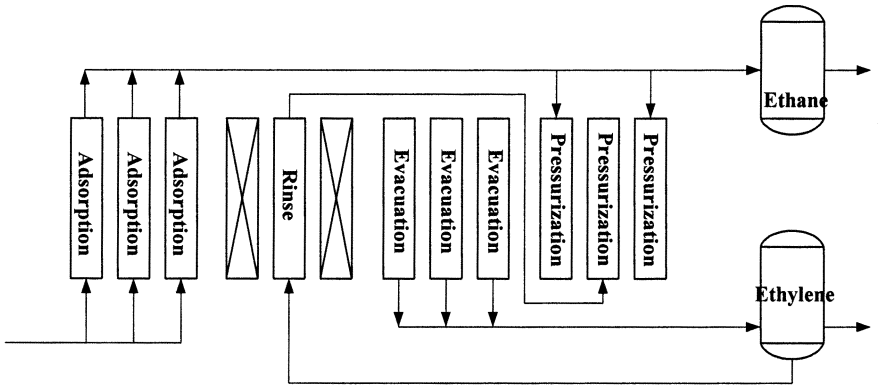

	30	110	10	30	110	10	30	110	10	30	110	10
A	Adsorption			Null	Rinse	Null	Evacuation			BF	Rinse-P	BF
B	BF	Rinse-P	BF	Adsorption			Null	Rinse	Null	Evacuation		
C	Evacuation			BF	Rinse-P	BF	Adsorption			Null	Rinse	Null
D	Null	Rinse	Null	Evacuation			BF	Rinse-P	BF	Adsorption		

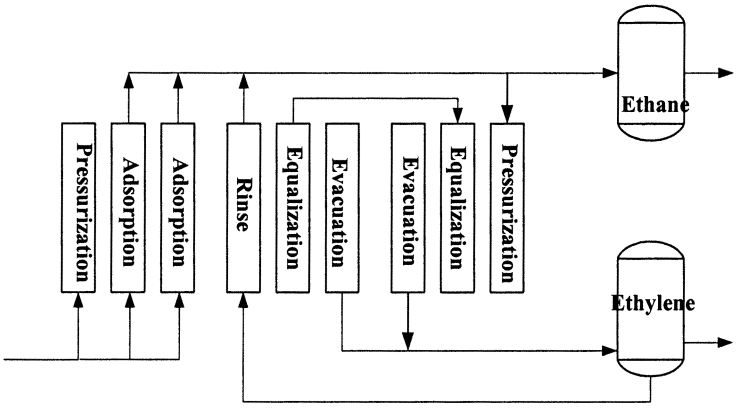

	40	60	5	45	40	60	5	45	40	60	5	45
A	FF	Adsorption			Rinse		EQ	Evacuation			EQ	BF
B	Evacuation		EQ	BF	FF	Adsorption			Rinse		EQ	EV
C	Rinse		EQ	Evacuation			EQ	BF	FF	Adsorption		

Fig. 2. Cycle configurations of the 4-bed and 3-bed VSA processes.
BF: Raffinate pressurization EQ: Pressure equalization EV: Evacuation FF: Feed pressurization

to pressurize the adsorber in the corresponding pressurization step. With this step, relatively high purity of ethylene in the effluent of the rinse step is recovered. On the other hand, in the 3-bed VSA process the effluent of the rinse step is vented to the ethane-rich stream.

MATHEMATICAL MODEL

The mathematical model adopted is a non-isothermal, non-equilibrium, bulk separation model. The assumption used to derive the model included the following: ideal gas behavior, no axial dispersion and no axial heat conduction, thermal equilibrium between gas phase and adsorbents. Mass transfer is represented by the linear driving force (LDF) approximation.

Based on the above assumptions, the mass balance for each component of the mixture and the total mass balance are written as follows:

Component mass balance:

$$\frac{\partial y_i}{\partial t} + u\frac{\partial y_i}{\partial z} + \frac{(1-\varepsilon)}{\varepsilon}\rho_p \frac{R_g T}{P}\frac{\partial \bar{q}_i}{\partial t} - y_i \sum_j \frac{(1-\varepsilon)}{\varepsilon}\rho_p \frac{R_g T}{P}\frac{\partial \bar{q}_i}{\partial t} = 0 \quad (1)$$

Total mass balance:

$$\frac{\partial C}{\partial t} + \frac{\partial (uC)}{\partial z} + \sum_i \frac{(1-\varepsilon)}{\varepsilon}\rho_p \frac{\partial \bar{q}_i}{\partial t} = 0 \quad (2)$$

Energy balance for the gas phase includes the heat transfer to the column wall:

$$(\varepsilon c_{pg} C + (1-\varepsilon) c_{ps}\rho_p)\frac{\partial T}{\partial t} + \varepsilon c_{pg} u C \frac{\partial T}{\partial z} - \sum_i (-\Delta H_a)_i (1-\varepsilon)\rho_p \frac{\partial \bar{q}_i}{\partial t} + \frac{2h_w}{R_i}(T - T_w) = 0 \quad (3)$$

In Eq. (3), the last term accounts for the heat transfer to the column

wall. The energy balance around the column wall is given by

$$c_{pw}\rho_w a_w \frac{\partial T_w}{\partial t} = 2\pi h_w R_i (T - T_w) - 2\pi U_w R_o (T_w - T_F) \quad (4)$$

Mass transfer is expressed by the LDF approximation.

$$\frac{\partial \bar{q}_i}{\partial t} = k_i (q_i^* - \bar{q}_i) \quad (5)$$

The steady state momentum balance is given by Ergun's equation:

$$-\frac{\partial P}{\partial z} = \frac{150\mu u}{d_p^2}\frac{(1-\varepsilon)^2}{\varepsilon^2} + 1.75\rho_g u^2 \frac{1-\varepsilon}{d_p \varepsilon} \quad (6)$$

In all simulations, it was assumed that the bed is saturated with pure ethane. Thereafter, the final conditions of the previous step become the initial conditions for the next step.

Boundary conditions for each step are written as follows.

Adsorption and rinse steps:

$$y_i(0,t) = y_{i,F}, \quad T(0,t) = T_F, \quad u(0,t) = u_H \quad (7a)$$

$$\left.\frac{\partial P}{\partial z}\right|_{z=0} = -K_1 u_H - K_2 u_H^2, \quad P(L,t) = P_H \quad (7b)$$

$$K_1 = \frac{150\mu}{d_p^2}\frac{(1-\varepsilon)^2}{\varepsilon^3}, \quad K_2 = 1.75\rho_g \frac{1-\varepsilon}{d_p \varepsilon^3}, \quad (7c)$$

EQ-BD step:

$$u(0,t) = 0 \quad u(L,t) = C_V(P|_{z=L} - P_{EQ-PR}) \quad (8)$$

Evacuation step:

$$u(L,t) = 0, \quad u(0,t) = u_S(1 - e^{-(P|_{t=0} - P_d)/a}) \quad u_S = Q/(A\varepsilon) \quad (9a)$$

$$u(L,t) =, \; P(0,t) = P(t) \quad (9b)$$

EQ-PR step:

$$y_i(L,t) = y_{i,EQ-BD}, T(L,t) = T_F \quad u(L,t) = u_{EQ-BD}\frac{P_{EQ-BD}}{P|_{z=L}} \quad (10)$$

FF step:

$$y_i(0,t) = y_{i,F} \quad T(0,t) = T_F \quad u(0,t) = u_H \quad (11)$$

Different boundary conditions were applied for the evacuation step according to the simulation purpose. For comparison between the simulation and experimental results, pressure histories obtained in the experiments were used as the boundary conditions of the evacuation step. In this case, piecewise quadratic interpolation of the experimental pressure history was used. In the parametric studies, gas velocity given by the Eq. (9a) was used for the boundary conditions. Pressure history at the evacuation step varies with the operating conditions and is not known prior to the experiment. In this case, specifying the velocity at the feed end makes the simulation much simpler.

It was assumed that the velocity of gas leaving the adsorber during the EQ-BD step, u_{EQ-BD}, was proportional to the pressure difference between product ends of two columns. Therefore, for the calculation of the velocity, information on the pressure history at the top of the column in the EQ-PR step, P_{EQ-PR}, was required. Assumed pressure history was used in the first cycle simulation. Thereafter, it was obtained from the simulation on the EQ-PR step. The adsorber characteristics with the heat and mass transfer coefficients and other constants used in the simulations are listed in Table 2.

Table 2. Physical parameters of adsorbent and adsorber

Physical properties of adsorbent and adsorber		
Bed length	(cm)	100
Bed diameter	(cm)	2.54
Bed porosity	(-)	0.36
Particle density	(g/cm^3)	1.84
Particle diameter	(cm)	0.15
Density of wall	(g/cm^3)	8.0
Heat capacity of gas	(cal/mol K)	8.0
Heat capacity of adsorbent	(cal/g K)	0.19
Heat capacity of wall	(cal/g K)	0.11
Heat and mass transfer coefficients		
h_w	(cal/cm^2 s K)	4.0×10^{-4}
U_w	(cal/cm^2 s K)	2.0×10^{-4}
$k_{C_2H_4}$	(s^{-1})	0.05
$k_{C_2H_6}$	(s^{-1})	0.1

Volume averaged recovery and purity were used as performance parameters. This is mathematically equivalent to the molar average because the ideal gas law was applied.

1. Adsorption Equilibrium

The adsorption isotherms of ethane can be represented by a conventional and simple adsorption isotherm model such as the Langmuir model. However, since the adsorption of ethylene takes places on two distinctive sites, $AgNO_3$ and clay surface, and the adsorption energies on these two sites are greatly different, it is reasonable to represent the adsorption isotherms of ethylene with the following two sites model, hybrid model of the Langmuir and Unilan isotherm [Yang and Kikkinides, 1995].

$$q_{C_2H_6}^* = \frac{q_{si} b_i p_i}{1 + b_i p_i} \quad (12)$$

$$q_{C_2H_4}^* = \frac{q_{si} b_i p_i}{1 + b_i p_i} + \frac{q_{sc}}{2s}\ln\left(\frac{1 + b_c p_i e^{s}}{1 + b_c p_i e^{-s}}\right) \quad (13)$$

where the parameters depend on the temperature in the following way:

$$b_i = b_{io}\exp(b_1/T), \; q_{si} = a_{i,1} + a_{i,2}/T, \quad (14a)$$

$$b_c = b_{co}\exp(b_{c1}/T), \; q_{si} = a_{i,1} + a_{i,2}/T, \; s = 1729/T \quad (14b)$$

The first term of RHS of Eq. (13) represents the physisorption and the second term represents the weak chemisorption, π-complexation. Five fitting parameters are involved in the model Eq. (13). If all the parameters are treated as true fitting parameters, the resulting parameters will lose physical significance. Yang et al. [1995] imposed constraints on q_{si} and b_i, and s. They used the Langmuir parameters of ethane as upper bounds for the Langmuir parameters of ethylene. In this study, it was assumed that the Langmuir parameters of ethylene were the same as those of ethane. By doing so, true fitting parameters were reduced to three. The isotherm parameters and the heats of adsorption are listed in Table 3.

The binary adsorption equilibrium of ethane/ethylene was represented by the following model.

Table 3. Isotherm parameters and heats of adsorption

	q_{mp} (mmol/g)	$b_o \times 10^7$ (1/mmHg)	b_1 (K)	$q_{sc,a}$ (mmol/g)	$q_{sc,b}$ (K)	$b_{sc,0}$ (1/mmHg)	$b_{sc,1}$ (K)	$-\Delta H$ (cal/mol)
C_2H_6	0.298	5.57	1,886					4,404
C_2H_4	0.298	5.57	1,886	2.175	0.290	1.31	2,352	8,817

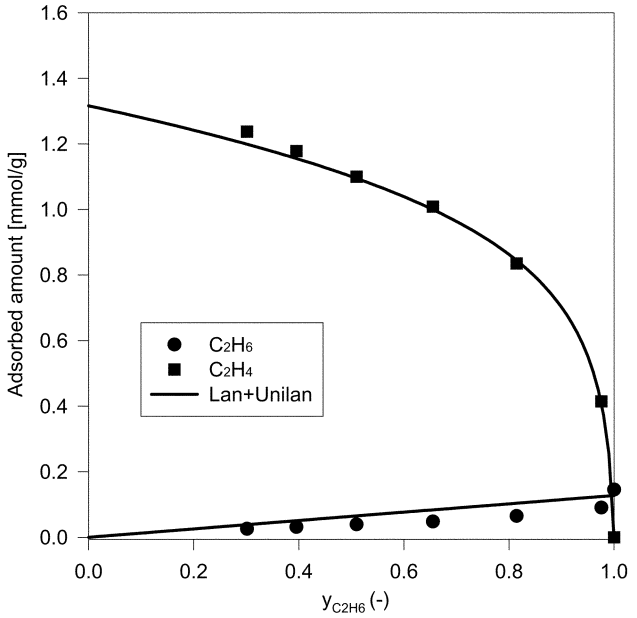

Fig. 3. Binary adsorption equilibrium of ethylene/ethane at 25 °C, 900 mmHg.

$$q^*_{C_2H_6} = \frac{q_{si} b_i p_i}{1 + \sum_j b_j p_j} \tag{15}$$

$$q^*_{C_2H_4} = \frac{q_{si} b_i p_i}{1 + \sum_j b_j p_j} + \frac{q_{sc}}{2s} \ln\left(\frac{1 + b_c p_i e^{s}}{1 + b_c p_i e^{-s}}\right) \tag{16}$$

The binary adsorption model is the extension of the pure component isotherm model. It is based on the assumption that the competitive adsorption of ethane/ethylene takes place only on the bare clay surface, and the surface site covered by $AgNO_3$ adsorbs only ethylene. Fig. 3 shows the binary adsorption equilibrium of ethane/ethylene on $AgNO_3$/clay at 25 °C and 900 mmHg. It is clear from Fig. 3 that the adsorption equilibrium model represents the amounts adsorbed of both components quite well. Minor discrepancy between the model and experiment for the amount adsorbed of ethane results from the assumption that ethane is not adsorbed on $AgNO_3$. Basically, there is a dispersion force between $AgNO_3$ and ethane so that ethane can also be adsorbed on $AgNO_3$. However, if the adsorption site, $AgNO_3$, is occupied by the strongly adsorbed component, ethylene, adsorption of ethane on $AgNO_3$ will be almost impossible. Rapid decrease of the amount adsorbed of ethane in the region where small amount of ethylene is in the gas phase can be interpreted as the result of competitive adsorption of ethylene and ethane on $AgNO_3$. After the rapid decrease of the amount adsorbed of ethane, it decreased almost linearly with the mole fraction of ethylene. As shown in Eq. (15), the amount adsorbed of ethane is a linear function of ethane partial pressure when both components have

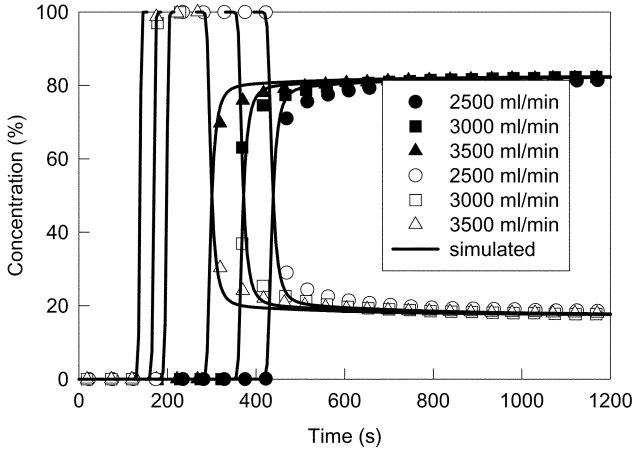

Fig. 4. Breakthrough curves of C_2H_4/C_2H_6 mixture on $AgNO_3$/clay bed with the feed flow rate (filled symbols: C_2H_4, empty symbols: C_2H_6).

the same Langmuir parameters. The linear decrease of the amount adsorbed of ethane confirms the assumption that the physisorption parameters of ethylene and ethane on bare clay surface are almost the same.

Since the competitive adsorption of ethylene and ethane on $AgNO_3$ is not taken into account in model Eqs. (15) and (16), the amount adsorbed of ethane is over-predicted. However, the difference between model and experimental data is not so large.

RESULTS AND DISCUSSION

1. Breakthrough Experiment

Fig. 4 shows the concentration breakthrough curves of ethane and ethylene with feed flow rate. Each experiment was performed with the completely regenerated adsorbent by purging with helium at 150 °C and vacuum. By doing so, completely reproducible breakthrough curves were obtained. As the feed flow rate increases, the breakthrough times of both components are getting short. Breakthroughs of both components take place very sharply. As shown in Fig. 4, the breakthrough curves of ethane and ethylene are predicted quite well by the mathematical model. Fig. 5 shows the temperature excursions at several points of the bed. Due to the heat released by the adsorption of ethylene and ethane, temperature excursion curves show two temperature plateaus that correspond to the adsorption of ethane and ethylene, respectively. When ethylene adsorption takes place, the bed temperature rises to 60 °C. The temperature excursions above 30 cm from feed end show only minor difference, which means that the concentration profiles in the bed reach a constant pattern above 30 cm. As shown in Fig. 5, all the general trends of the temperature variation are well predicted by the model.

The mass transfer coefficient of ethylene which best fitted the

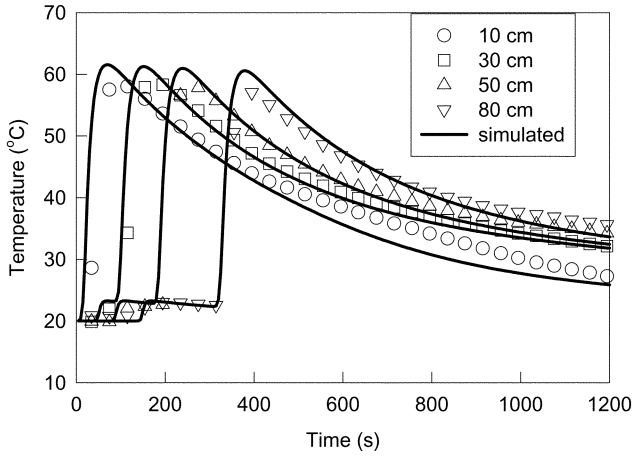

Fig. 5. Temperature excursions at several positions of the adsorber (Feed flow rate: 2,500 ml/min, adsorption pressure: 1,100 mmHg).

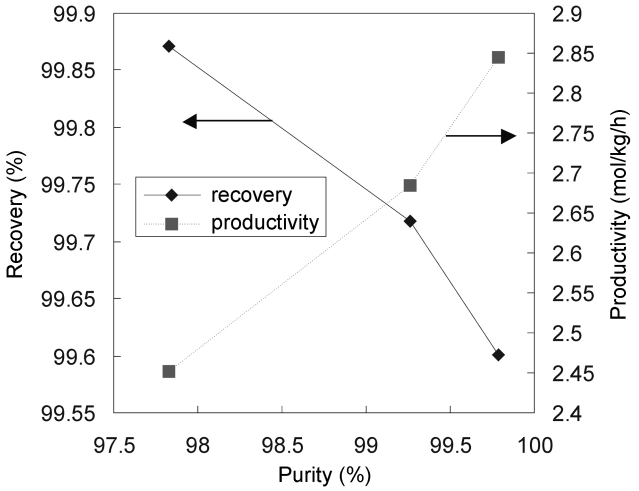

Fig. 6. Performance of the 4-bed VSA process (feed: C2 fractionator feed 83.56% C_2H_4/16.44% C_2H_6).

experimental breakthrough curves was 0.051/s. There was some uncertainty for the mass transfer coefficients of ethane since the breakthrough of ethane occurred abruptly. According to the simulation results, mass transfer coefficients of ethane from 0.05 s^{-1} to 0.2 s^{-1} gave almost the same breakthrough curves for ethane.

2. Comparison of 4-bed and 3-bed VSA Process

The 4-bed VSA process has been widely accepted for the olefin separation [Cho et al., 2002; Rege and Yang, 2002]. This is partly due to the market price of ethylene. Since the market price of ethylene is high, a process of high recovery has been preferred. The adsorptive separation process for enriching the strongly adsorbed component often employs a rinse step, purging the adsorber with the strongly adsorbed component. In the 4-bed VSA process, the ethylene vented during the rinse step can be recycled to another adsorber without interruption as shown in Fig. 2. Since the loss of ethylene during the rinse step can be reduced in the 4-bed VSA process, it is suitable for the process where high recovery is the major concern.

Not only the recovery but also the productivity is an important performance criterion of the adsorptive separation process. The productivity becomes more important for a process that requires high investment cost. The π-complexation adsorbent used in this study contains a noble metal, Ag, so that the cost of $AgNO_3$/clay and the investment cost of the process would be high. This makes the productivity another important performance criterion of the process using the π-complexation adsorbent. A simple way to reduce the investment cost and hence to improve the process economics is by employing a smaller number of adsorbers.

Here, the performances of 4-bed and 3-bed VSA process are compared especially with respect to the productivity. Fig. 6 shows the performance of the 4-bed VSA process. In all experiments, the adsorption and desorption pressures were 1,200 mmHg and 20 mmHg, respectively. The performance of the 4-bed VSA process shown in Fig. 6 was obtained by varying the feed flow rate from 2,500 ml/min to 3,000 ml/min. Therefore, the highest product purity shown in Fig. 6 was obtained at a feed flow rate of 3,000 ml/min. As shown in Fig. 6, the recoveries of the 4-bed VSA process were over 99% at all feed flow rates. At a feed flow rate of 3,000 ml/min, the purity

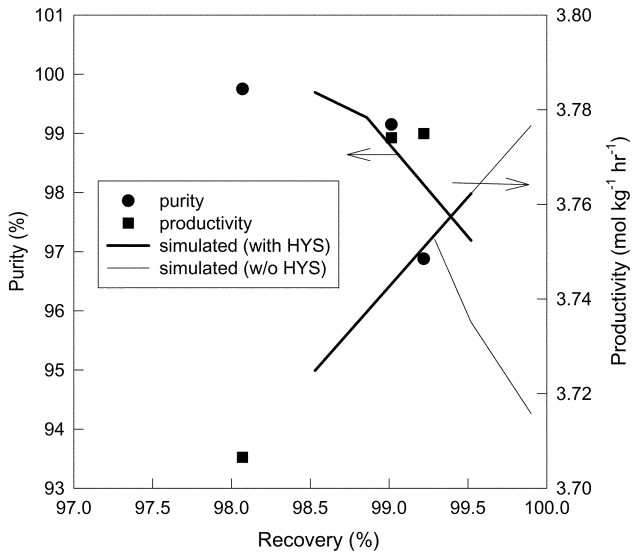

Fig. 7. Performances of the 3-bed VSA process (bold lines: isotherm accounting for the hysteresis, sharp lines: isotherm from fresh adsorbent).

and recovery of ethylene were 99.85%, 99.6%, respectively.

The performance of the 3-bed VSA process is shown in Fig. 7. The adsorption and desorption pressure were the same as in the 4-bed VSA process. The feed flow rate was fixed at 3,000 ml/min. Performance shown in Fig. 7 was obtained by varying the duration of the pressure equalization step. The lowest purity of the 3-bed VSA process shown in Fig. 7 corresponds to the cycle operated without the pressure equalization step. Without the pressure equalization step, ethylene purity of 96.5% was produced with a recovery of 99.2%. Compared with the 4-bed VSA process, the purity is much lower than the 4-bed VSA, where 99.8% ethylene is produced at a feed flow rate of 3,000 ml/min. This was because the rinse flow rate of the 3-bed VSA process was lower than that of the 4-bed VSA process. The rinse flow rates of the 4-bed and 3-bed VSA process were 800 ml/min and 685ml/min, respectively.

In the 3-bed VSA process, one more step is included: pressure

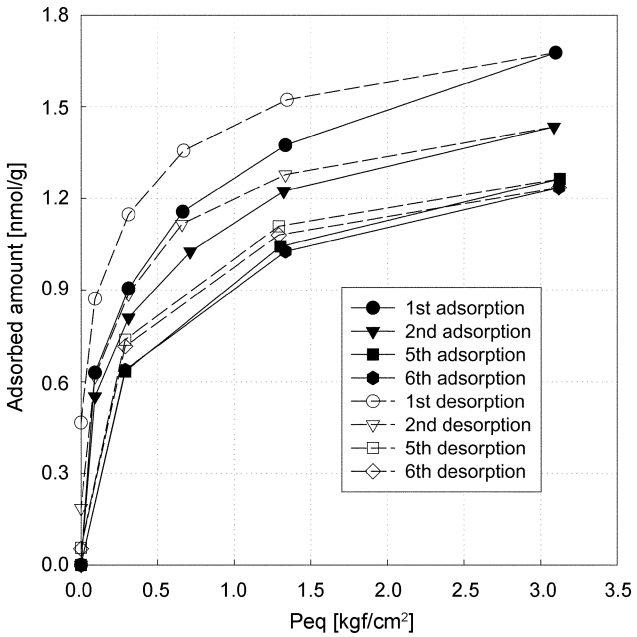

Fig. 8. Adsorption-desorption isotherms of ethylene at 25 °C from repeated adsorption and desorption isotherm measurement.

equalization step. During the pressure equalization step, the weakly adsorbed component, ethane, is preferentially desorbed so that higher purity of ethylene is produced in the subsequent desorption step. When the pressure equalization time increased to 5 s and 10 s, the product purity increased 99.2% and 99.8%, respectively. The performance of the 3-bed VSA is better than the 4-bed process in the sense that it gives high productivity. At a purity of 99.8%, the productivities of the 4-bed and 3-bed VSA process were 2.8 mol/kg/hr and 3.7 mol/kg/hr, respectively. That is, productivity was improved about by 33% compared to the 4-bed VSA process.

3. Simulation of the 3-bed VSA Process

The 3-bed VSA process was superior to the 4-bed VSA process in the sense that it gives high productivity. Simulation was performed for the 3-bed VSA process. The adsorbent used in this study showed some degree of hysteresis. Fig. 8 shows the adsorption and desorption isotherms obtained during the repeated adsorption-desorption equilibrium measurement. The experiment started with the completely regenerated adsorbent and then continued without complete regeneration in the subsequent measurements, which is the real situation occurring in the cycle operation. The amounts adsorbed of the adsorption isotherms shown in Fig. 8 are the net adsorption amount obtained after the residual adsorption amount of the previous desorption measurement is subtracted from the total adsorption amount. In the first adsorption-desorption isotherm measurement, a large gap between the adsorption and desorption isotherm was observed, and the residual adsorption amount at ultimate vacuum was about 0.5 mmol/g. However, not only the gap between the adsorption and desorption isotherm but also the residual adsorption amount became small as the measurements proceeded. At the second adsorption-desorption isotherm measurement, the residual adsorption amount was about 0.15 mmol/g. The hysteresis did not completely disappear even at the 5th and 6th measurements. But, the adsorption and desorption isotherms were reproducible from the 5th adsorption-desorption isotherm measurement. It is seen in Fig. 8 that the adsorption and desorption isotherms from the 5th measurement are almost the same as those from the 6th measurement.

The adsorption amounts at the 5th and 6th measurement were about 80% of that at the first measurement, especially below 1,200 mmHg, the adsorption pressure of the VSA experiment.

With these results in hand, different from the breakthrough simulations where an isotherm from the fresh adsorbent was applied, process simulations were performed under the assumption that the reversible adsorption amount of ethylene was 80% of that obtained from the fresh adsorbent. That assumption was incorporated by multiplying 0.8 to the adsorption isotherm of ethylene obtained from the fresh adsorbent. The results are shown in Fig. 7. The bold lines in Fig. 7 represent the simulation results when the isotherm that takes into account the hysteresis is applied. Simulation quite well predicted the experimental results. Minor discrepancy between the experiment and simulation is unavoidable because of the inaccuracy of the isotherm used.

For comparison, the simulation results with the isotherm obtained from the fresh adsorbent are also shown in Fig. 7. Sharp lines in Fig. 7 represent the simulation results when the isotherm from the fresh adsorbent is applied. As shown in Fig. 7, while the purity from the simulation was 2% lower than that from the experiment, the recovery from the simulation was higher than that from the experiment. This is because the hysteresis is not properly accounted for in the isotherm.

In Fig. 9, the temperature profiles at 80 cm from the feed inlet are compared with the simulation results. The experimental temperature profile was obtained at a pressure equalization time of 5 s. When the hysteresis is accounted for in the isotherm, the temperature profiles are well predicted. But, when the hysteresis is not accounted for, the simulated temperature profile reaches its maximum at the end of the rinse step. This means that the concentration front reaches 80 cm at the end of the rinse step. This is because the adsorption amount of ethylene is over-predicted in the simulation.

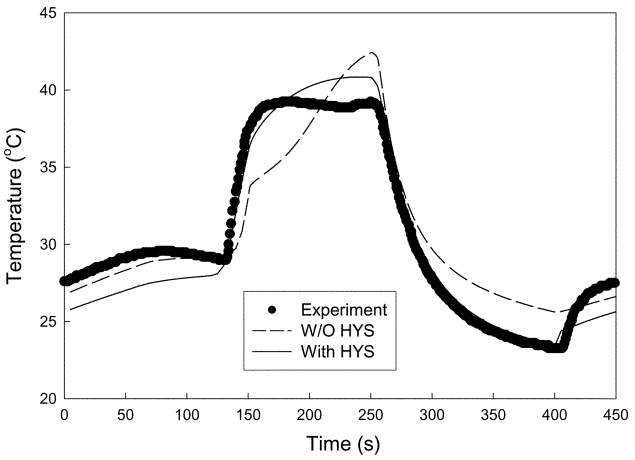

Fig. 9. Simulated and experimental temperature profiles at 80 cm from the feed inlet (feed: 3,000 ml/min, rinse: 685 ml/min, desorption pressure: 20 mmHg) (Solid line: isotherm accounting for hysteresis, dotted line: isotherm from fresh adsorbent).

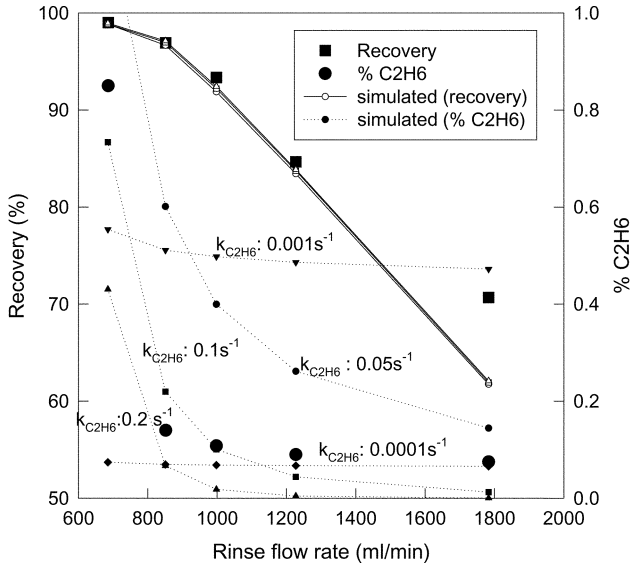

Fig. 10. Recovery and impurity concentration of the 3-bed VSA process with the rinse flow rate. Simulations are performed with different mass transfer coefficients of ethane (Feed: 3,000 ml/min, EQ step time: 5 s).

4. Effects of Rinse Flow Rate

Though ethylene purity of 99.8% is sufficient for most applications, ethylene purity of over 99.9% is often requested by industry. One way of producing such a high purity of ethylene is to rinse the bed with product ethylene. During this rinse step, a weakly adsorbed component in the bed void and adsorbent is washed out of the adsorber by the strongly adsorbed component. So, high purity of strongly adsorbed component is obtained in the subsequent desorption step. In order to identify the amount of rinse gas for high purity ethylene production, experiments were performed varying the rinse flow rate. The results are shown in Fig. 10. The rinse flow rate was varied from 700 to 1800 ml/min. When the rinse flow rate was increased from 700 ml/min to 1,500 mL/min, the recovery was decreased from 98% to 70% because of the loss of ethylene during the rinse step. However, the concentration of impurity fell at first and then it was almost constant above the rinse flow rate of 800 ml/min. Even when the recovery was 70%, the concentration of impurity was 0.08%.

This may be attributed to the slow diffusion of ethane. To verify this, simulations were performed varying the mass transfer coefficients of ethane. The results are compared with the experimental results in Fig. 10. The change of recovery with the rinse flow rate was well predicted by the simulation. The recovery was not significantly affected by the mass transfer coefficient of ethane when the other operating conditions were the same. However, the purity of ethylene was greatly affected by the mass transfer coefficient of ethane. When the mass transfer coefficient of ethane was 0.2 s^{-1}, the concentration of impurity readily fell below 0.1%. However, when the mass transfer coefficient of ethane was 0.05 s^{-1}, the concentration of impurity was 0.2% even when the recovery fell below 65%.

When the mass transfer coefficient of ethane is 0.2 s^{-1}, ethane adsorbed during the adsorption and pressurization steps is easily desorbed by rinsing the adsorber with ethylene. Therefore, the concentration of impurity, ethane, in the product is readily reduced increasing the rinse flow rate. However, when the mass transfer coefficient of ethane is 0.05 s^{-1}, less amount of ethane is desorbed during the rinse step. Because of this, high purity of ethylene is not readily obtained when the mass transfer coefficient is 0.05 s^{-1}.

When the mass transfer is further reduced to 0.001 s^{-1}, the concentration of ethane in the product is nearly constant regardless of the rinse flow rate. This means that the rinse step does not play its function to replace ethane. At a mass transfer coefficient of 0.0001 s^{-1}, it is still true that the rinse step is not able to increase the product purity. However, in this case the concentration of the impurity is lower than that at the mass transfer coefficient of 0.001 s^{-1}. This is because the amount of ethane adsorbed during the adsorption and pressurization steps becomes small at this order of mass transfer coefficient.

It is noted that the mass transfer coefficient of 0.1 s^{-1} for ethane best predicts the experimental results. Since the diffusion time constant of ethane was 9.8×10^{-3} s^{-1} [Choudary et al., 2002], the value of the mass transfer coefficient for ethane is reasonable.

5. Effects of Feed Flow Rates

If the feed flow rate is increased, the productivity could be increased at the expense of the recovery. Fig. 11 shows the simulation results for the process performance with the feed flow rate. In the simulations, the adsorption and desorption pressure were fixed at 1,200 mmHg and 20 mmHg, respectively. Each curve was obtained by varying the rinse flow rate. The amount of feed introduced during the adsorption step was kept constant by adjusting the adsorption step time.

At the ethylene purity of 99.5%, the productivities of the process at the feed flow rate of 3,000 ml/min, 4,000 ml/min, 5,000 ml/min were 3.7 mol/kg/hr, 4.7 mol/kg/hr, 5.2 mol/kg/hr, respectively. When the feed flow rate increased from 3,000 ml/min to 4,000 ml/min, the recovery decreased only by 3% with a productivity increase

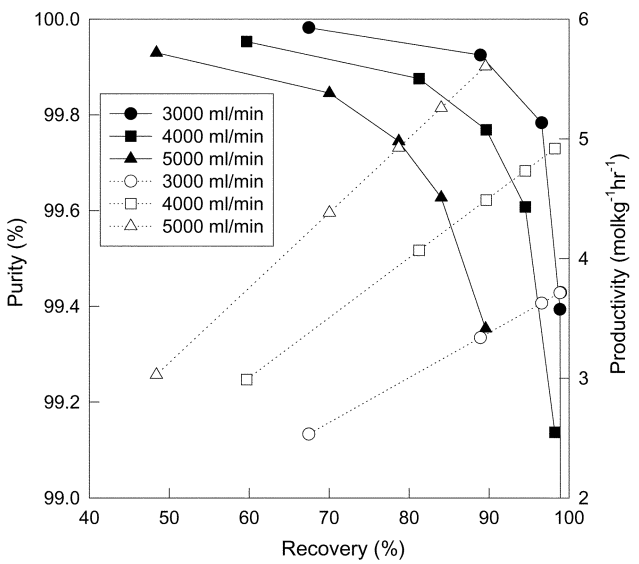

Fig. 11. Performances of the 3-bed VSA process with the feed flow rate (Adsorption pressure: 1,200 mmHg, Desorption pressure: 20 mmHg, black symbols: purity, blank symbols: productivity).

of 1 mol/kg/hr. That is, the increase of productivity is much more significant compared to the decrease of the recovery. However, when the feed flow rate increased from 4,000 ml/min to 5,000 ml/min, the recovery of the process fell about 7% with the increase of the productivity by 0.5 mol/kg/hr.

CONCLUSIONS

The performance of the 4-bed and 3-bed VSA process using $AgNO_3$/clay adsorbent for the ethylene separation from C2 fractionator feed (83.56% C_2H_4, 16.44% C_2H_6) was investigated experimentally and theoretically. The productivity of the 3-bed VSA was higher by about 33% than that of the 4-bed VSA at the ethylene purity of 99.8%. However, the recovery of the 3-bed VSA was marginally lower than that of the 4-bed VSA process due to the loss of ethylene during the rinse step.

Effects of the rinse flow rate in the 3-bed VSA process were investigated by both experiment and simulation. The purity of ethylene was not significantly improved by the increase of the rinse flow rate after it reached 99.8%. At the rinse flow rate where the purity was 99.9%, the recovery became 70%. It was probably because of slow diffusion of ethane. When the diffusion rate of ethane was low, ethane adsorbed during the adsorption and pressurization steps was not desorbed by ethylene at the rinse step. This contaminated the product ethylene at the subsequent desorption step. If the mass transfer coefficient was further reduced below 0.001 s^{-1}, then the product purity was not improved by rinsing with product ethylene under the operating conditions studied here.

According to the simulation, ethylene purity of over 99.9% could be obtained with recovery of over 90% only when the mass transfer rate of ethane was lower than 1.0×10^{-4} s^{-1} or higher than 0.2 s^{-1}. Effects of feed flow rate were investigated by simulation. According to the simulation, at a feed flow rate of 5,000 ml/min, productivity of 5.2 mol/kg/hr was obtained at an ethylene purity of 99.5%.

ACKNOWLEDGMENT

This research was supported by Korea Institute of Science & Technology Evaluation and Planning (KISTEP) under National Research Laboratory (NRL) program.

NOMENCLATURE

a : parameter defined in Eq. (8) [mmHg]
a_w : cross-sectional area of column wall [cm^2]
b_c : Unilan isotherm parameter [1/mmHg]
b_i : Langmuir isotherm parameter [1/mmHg]
C : gas phase concentration [mol/cm^3]
c_{pg} : heat capacity of gas phase [cal/mol K]
c_{ps} : heat capacity of particle [cal/g K]
c_{pw} : heat capacity of column wall [cal/g K]
C_V : valve coefficient [-]
d_p : diameter of particles [cm]
h_w : heat transfer coefficient at inner column wall [cal/cm^2 s K]
$(-\Delta H_a)_i$: heat of adsorption of i th component [cal/mol]
k_i : mass transfer coefficient of i th component [1/s]
K_1 : parameter defined in Eq. (7c)
K_2 : parameter defined in Eq. (7c)
P : pressure [mmHg]
P_d : the lowest desorption pressure [mmHg]
Q : suction capacity of vacuum pump [cm^3/s]
q_i^* : equilibrium amount adsorbed [mol/g]
$\bar{q}_i$: amount adsorbed of i th component [mol/g]
q_{sc} : Unilan parameter in Eq. (13) [mol/g]
q_{si} : saturation amount adsorbed of i th component [mol/g]
R_i, R_o: inner and outer radius of column [cm]
R_g : gas constant
s : Unilan parameter [-]
t : time [s]
T : gas phase temperature [K]
T_F : feed temperature [K]
T_w : wall temperature [K]
u : interstitial velocity [cm/s]
u_H : interstitial velocity of feed [cm/s]
u_{PU} : purge gas velocity [cm/s]
U_w : wall heat transfer coefficient at outer surface [cal/cm^2 s K]
y_i : mole fraction of i th component in the gas phase
$y_{i,AD}$: composition of ith component in the adsorption effluent
$y_{i,EQ\text{-}BD}$: composition of ith component in the effluent of the EQ-BD step
$y_{i,F}$: composition of ith component in the feed
z : the distance along the length of the column [cm]

Greek Letters

ε : bed void fraction
μ : gas viscosity [cP]
ρ_g : gas density [g/cm^3]
ρ_p : density of particles [g/cm^3]
ρ_w : density of wall [g/cm^3]

REFERENCES

Cen, P. L., "Simultaneous Physical and Chemical Adsorption of Ethylene and Cu(I) NaY Zeolite," Fundamentals of Adsorption, Mersmann, A. B. and Scholl, S. E. eds., Engineering Foundation, New York, 191 (1991).

Chen, J. P. and Yang, R. T., "Molecular Orbital Study of Selective Adsorption of Simple Hydrocarbons on Ag^+ and Cu^+ Exchanged Resins and Halides," *Langmuir*, **11**, 3450 (1995).

Cheng, L. S. and Yang, R. T., "Monolayer Cuprous Chloride Dispersed on Pillared Clays for Olefin-Paraffin Separations by π-Complexation," *Adsorption*, **1**, 61 (1995).

Cho, S. H., Han, S. S., Kim, J. N., Choudary, N. V., Kumar, P. and Bhat, S. G. T., "Light Olefin/Paraffin Separation by Vacuum Swing Adsorption Process," 1999 AIChE Annual Meeting, Dallas, TX, Oct. 31-Nov. 5, T1027-PSA/TSA I (1999).

Cho, S. H., Han, S. S., Kim, J. N., Choudary, N. V., Kumar, P. and Bhat, S. G. T., "Adsorbents and Methods for the Separation of Ethylene and Propylene and/or Unsaturated Hydrocarbons from Mixed Gases," Korean Patent, 0279881 (2000).

Cho, S. H., Han, S. S., Kim, J. N., Choudary, N. V., Kumar, P. and Bhat, S. G. T., "Adsorbents, Methods for the Preparation and Method for the Separation of Unsaturated Hydrocarbons for Mixed Gases," US Patent, 6315816 B1 (2001).

Cho, S. H., Han, S. S., Kim, J. N., Park, J. H. and Rhee, H. K., "Adsorptive Ethylene Recovery from LDPE Off-Gas," *Korean J. Chem. Eng*., **19**(5), 821 (2002).

Choi, W. K., Kwon, T. I., Yeo, Y. K., Lee, H., Song, H. K. and Na, B. K., "Optimal Operation of the Pressure Swing Adsorption (PSA) Process for CO_2 Recovery," *Korean J. Chem. Eng*., **20**(4), 617 (2003).

Choudary, N. V., Kumar, P., Bhat, S. G. T., Cho, S. H., Han, S. S. and Kim, J. N., "Adsorption of Light Hydrocarbon Gases on Olefin Selective Adsorbent," *Ind. Eng. Chem. Res*., **41**, 2728 (2002).

Cotton, F. A. and Wilkinson, G., "Advanced Inorganic Chemistry," 2nd ed., Chaps 25 and 28, Interscience, New York (1966).

Gilliland, E. R., Bliss, H. L. and Kip, C. E., "Reaction of Olefin with Solid Cuprous Halide," *J. Amer. Chem. Soc*., **63**, 2088 (1941).

Han, S. S., Kim, J. N., Cho, S. H., Choudary, N. V., Kumar, P. and Bhat, S. G. T., "Adsorbents for Light Alkane/Alkene Separation," The 8th APPChE Congress, Aug. 16-19, Seoul, Korea, 1777 (1999).

Hirai, H., "Polymers Complex for the Separation of Carbon Monoxide and Ethylene," Polymers for Gas Separation, Chap. 7, Toshima, N. ed., VCH Publishers, New York, 221 (1992).

Hirai, H., Hara, S. and Komiyama, M., "Polystyrene-Supported Aluminum Silver Chloride as a Selective Ethylene Adsorbent," *Angew. Makromol. Chem*., **130**, 207(1985).

Ho, W. S., Doyle, G., Savage, D. W. and Pruett, R. L., "Olefin Separations via Complexation with Cuprous Diketonate," *Ind. Eng. Chem. Res*., **27**, 334 (1988).

Keller, G. E., Marcinkowsky, A. E., Verma, S. K. and Williamson, K. D., "Olefin Recovery and Purification via Silver Complexation," Separation and Purification Technology, Chap. 3, Li, N. N. and Calo, J. M. eds., Dekker, New York (1992).

King, C. J., "Separation Process Based on Reversible Chemical Complexation," Handbook of Separation Process Technology, Rousseau, R. W. ed., Chap. 15, Wiley, New York (1987).

Ramachandran, R., Dao, L. H. and Brook, B., "Method Producing Unsaturated Hydrocarbons and Separating the Same from Saturated Hydrocarbons," US Patent, 5365011 (1998).

Rege, S. U., Padin, J. and Yang, R. T., "Olefin/Paraffin Separations by Adsorption: π-Complexation vs. Kinetic Separation," *AIChE J*., **44**(4), 799 (1999).

Rege, S. U. and Yang, R. T., "Propane/Propylene Separation by Pressure Swing Adsorption: Sorbent Comparison and Multiplicity of Cyclic Steady States," *Chem. Eng. Sci*., **57**, 1139 (2002).

Wu, Z., Han, S. S., Cho, S. H., Kim, J. N., Chue, K. T. and Yang, R. T., "Modification of Resin-Type Adsorbents for Ethane-Ethylene Separation," *Ind. Eng. Chem. Res*., **36**, 2749 (1997).

Yang, R. T. and Kikkinides, E. S., "New Sorbents for Olefin/Paraffin Separations by Adsorption via π-Complexation," *AIChE J*., **41**(3), 509(1995).